Journal of Engineering Mathematics **40:** 227–248, 2001.

The unsteady motion of two-dimensional flags with bending stiffness

A.D. FITT and M.P. POPE
Faculty of Mathematical Studies, University of Southampton, SO17 1BJ, U.K.

Received 1 July 1999; accepted in revised form 1 August 2000

Abstract. The motion of a two-dimensional flag at a time-dependent angle of incidence to an irrotational flow of an inviscid, incompressible fluid is examined. The flag is modelled as a thin, flexible, impermeable membrane of finite mass with bending stiffness. The flag is fixed at the leading edge where it is assumed to be either freely hinged or clamped with zero gradient. The angle of incidence to the outer flow is assumed to be small and thin aerofoil theory and simple beam theory are employed to obtain a partial singular integro-differential equation for the flag shape. Steady solutions to the problem are calculated analytically for various limiting cases and numerically for order one values of a non-dimensional parameter that measures the relative importance of outer flow momentum flux and flexural rigidity. For the unsteady problem, the stability of steady solutions depends only upon two non-dimensional parameters. Stability analysis is performed in order to identify the regions of instability. The resulting quadratic eigenvalue problem is solved numerically and the marginal stability curves for both the hinged and the clamped flags are constructed. These curves show that both stable and unstable solutions may exist for various values of the mass and flexural rigidity of the membrane and for both methods of attachment at the leading edge. In order to confirm the results of the linear stability analysis, the full unsteady flag equation is solved numerically using an explicit method. The numerical solutions agree with the predictions of the linear stability analysis and also identify the shapes that the flag adopts according to the magnitude of the flexural rigidity and mass.

Key words: unsteady incompressible aerodynamics, singular integro-differential equations, asymptotics, numerics, stability.

1. Introduction

This study analyses the motion of a two-dimensional flexible sheet, hereafter referred to as a 'flag', in an irrotational flow of an inviscid, incompressible fluid. The flag is modelled as a thin membrane of finite mass which has finite bending stiffness and is impermeable to the outer flow. The flag is fixed at its leading edge, and is free to move under the influence of the outer flow. We assume throughout that the angle of incidence of the outer flow is a prescribed function of time and is 'small' (in a sense that will be made clear below) thus permitting the flag, whose position will be denoted by $S(x, t)$, to be modelled using thin aerofoil theory. A schematic diagram of the flag is presented in Figure 1.

Many industrial processes involve the motion of flexible elastic fibres and sheets at small incidence to an air or liquid flow. Such circumstances are especially prevalent in textile manufacture. However, in spite of the obvious industrial applications, very little seems to have been published on any aspect of flag motion.

Haselgrove [1] analysed the unsteady motion of a flag of zero mass with no bending stiffness, concluding that it was unstable to small, time-dependent perturbations. Everyday observation of fluttering flags confirms this instability; without bending stiffness the trailing edge of a flag inevitably 'rolls up' in an unstable manner. Lattimer [2] (who primarily analysed

the unsteady, two-dimensional sail; a flag fixed at both ends) proposed an equation for a flag of non-zero mass, but did not consider the effects of bending stiffness and proceeded no further with the analysis. The fluttering of fibres in an airspinning process was examined by Bäcker *et al.* [3]. Their model assumed that the fibres were elastic and was fully nonlinear; they were only able to proceed numerically. The motion of an elastic panel embedded in an infinite rigid plane was investigated both theoretically and experimentally by Kornecki *et al.* [4]. They examined only plates with clamped or simply-supported leading edges, but were able to determine under what conditions unstable flutter might occur. They also studied the behaviour of an elastic panel with a parallel flow over both sides experimentally. The model proposed in this study is related to that considered in [4], but includes the effects of an angle of attack. A completely different method of solution is also adopted, and numerical results are provided for a much wider range of parameters. The analysis of [4] was extended in [5], and [6] further considered the flutter of cantilevered plates in axial flow.

This study proposes a model of unsteady flag motion that includes both finite mass and bending stiffness. Standard beam theory and thin aerofoil theory are used to derive a partial singular integro-differential equation that governs the motion when the flag is either clamped or hinged at its leading edge. The case of the steady flag, where the angle of incidence is constant, is analysed first. A numerical method is presented for both hinged and clamped flags and results are presented that show the effects of varying both the angle of incidence and the flexural rigidity of the flag.

The unsteady problem is then considered. In order to determine whether or not the steady solutions that have been calculated might ever be observed in practice, a linear stability analysis is performed. Marginal stability curves are presented for both methods of attachment at the leading edge; they indicate how the mass and flexural rigidity of the flag must be related for stability.

An explicit scheme for the unsteady flag equation is then presented and Von Neumann stability analysis is performed to determine under what conditions the method is stable. Results are then presented for both hinged and clamped flags; the resulting behaviour agrees with the linear stability analysis. Throughout, a number of limiting cases are also examined.

2. Derivation of the unsteady flag equation

We analyse the irrotational flow of an inviscid, incompressible fluid past a two-dimensional flag at angle of incidence $\alpha(t)$. The speed of the undisturbed free stream is denoted by U_∞. The flag, whose position is denoted by $S(x, t)$, is fixed at $x = 0$ and has length L; the free end is situated at $S(c, t)$ where $c < L$, as depicted in Figure 1. We write the stream function ψ and velocity potential ϕ as

$$\psi(x, y, t) = yU_\infty \cos\alpha(t) - xU_\infty \sin\alpha(t) + \frac{1}{2\pi}\int_0^\infty \frac{f(\eta, t)}{2} \log\left((x-\eta)^2 + y^2\right) \mathrm{d}\eta, \quad (1)$$

$$\phi(x, y, t) = xU_\infty \cos\alpha(t) + yU_\infty \sin\alpha(t) - \frac{1}{2\pi}\int_0^\infty f(\eta, t)\theta(x, y, \eta)\mathrm{d}\eta, \quad (2)$$

where $\tan\theta = y/(x-\eta)$ and f is to be determined. As yet, we have made no assumptions about the orders of magnitude of the terms in (1) and (2), though we have anticipated the form of what is to come by expressing (1) and (2) as the sum of an angled free stream and a

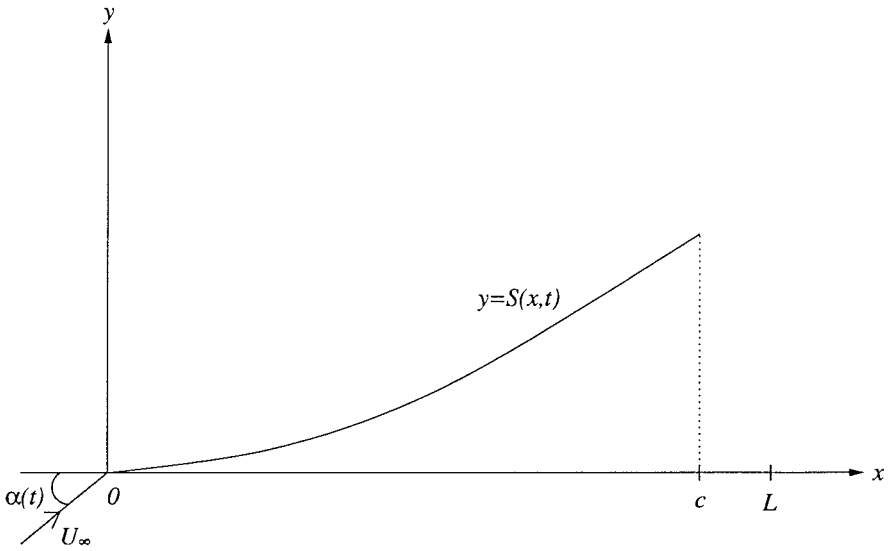

Figure 1. Schematic diagram of a flag.

distribution of vortices. We assume that the flag is impermeable (the effects of gravity and flag porosity could easily be included if required) so that $(\mathrm{D}/\mathrm{D}t)[y - S(x,t)] = 0$ at $y = S(x,t)$. Thus

$$S_t + \psi_y S_x = -\psi_x \quad \text{at} \quad y = S(x,t). \tag{3}$$

Since the flow is irrotational, the unsteady Bernoulli equation applies. Thus the quantity

$$\phi_t + \frac{p}{\rho} + \frac{1}{2}(\psi_x^2 + \psi_y^2)$$

(where p and ρ denote, respectively, the fluid pressure and density) is a function of time alone.

We seek to examine only cases where the angle of attack of the oncoming stream is small and the resultant deflection of the flag is therefore also small. The key small parameter ϵ in the problem is thus defined by the order of magnitude of α. Accordingly, we non-dimensionalise using $x = Lx^*$, $\eta = L\eta^*$, $y = Ly^*$, $S = \epsilon L S^*$, $\alpha = \epsilon\alpha^*$, $f = \epsilon U_\infty f^*$, $\psi = LU_\infty\psi^*$ and $t = (L/U_\infty)t^*$, where a star denotes a non-dimensional quantity. The non-dimensionalisation amounts to invoking standard 'thin-aerofoil' theory, and the stream function and velocity potential now represent an angled free stream perturbed (since the flag has zero thickness but generates a non-zero lift) by a distribution of vortices.

To leading order, we find that (3) should now be imposed on $y^* = 0$. Here, the derivatives of the stream function are given by

$$\lim_{y^*\to 0^\pm}(\psi^*_{y^*}) = 1 \pm \frac{\epsilon}{2} f^*(x^*,t^*), \quad \lim_{y^*\to 0}(-\psi^*_{x^*}) = \epsilon\alpha^*(t^*) - \frac{\epsilon}{2\pi}\int\!\!\!\!\!\!-_0^\infty \frac{f^*(\eta^*,t^*)}{x^*-\eta^*}\mathrm{d}\eta^*, \tag{4}$$

where as usual a bar through the integral sign denotes a Cauchy Principal value. The kinematic condition (3) thus shows that $S(x,t)$ satisfies

$$S^*_{t^*} + S^*_{x^*}\left(1 + \frac{\epsilon}{2} f^*(x^*,t^*)\right) = \alpha^*(t^*) - \frac{1}{2\pi}\int\!\!\!\!\!\!-_0^\infty \frac{f^*(\eta^*,t^*)}{x^*-\eta^*}\mathrm{d}\eta^*. \tag{5}$$

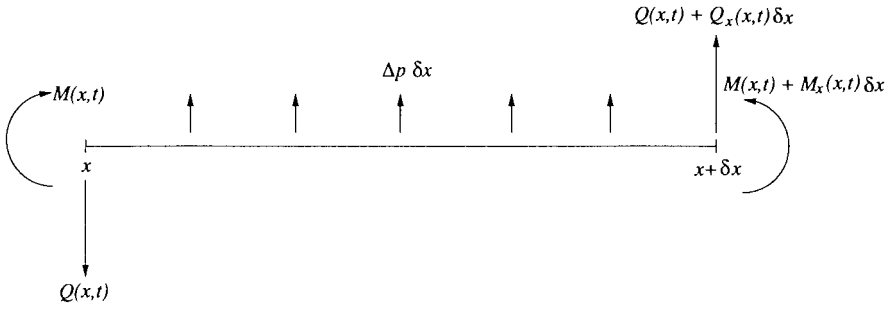

Figure 2. The forces acting on a flag element.

In order to determine $f^*(x^*, t^*)$ in terms of $S^*(x^*, t^*)$ and close the problem it is necessary to analyse the forces acting upon the flag. Standard beam theory is employed to analyse the inclusion of bending stiffness in the flag. Following (for example) [7] we assume that the rotation of the beam is insignificant compared to the vertical translation, and that the shear deformation is small compared to the bending deformation.

We work in dimensional variables for the present and denote the mass per unit length and the flexural rigidity of the flag (measured in kg/m^2 and kg m^2/s^2) by ρ' and γ respectively. As γ increases, the flag's ability to bend is restricted since more force is required per unit length to produce the same vertical displacement. Figure 2 depicts the forces acting on a flag element of length δx. $Q(x, t)$ denotes the shearing force, $M(x, t)$ is the bending moment and $\Delta p = p_- - p_+$ is the pressure difference across the flag. If we apply Newton's Second Law to the flag element in the vertical direction we find that

$$(Q + Q_x\delta x) - Q + \Delta p\delta x = \rho'\delta x S_{tt}$$

and thus

$$Q_x + \Delta p = \rho' S_{tt}. \tag{6}$$

If we now take moments about x (denoting anti-clockwise moments as positive), we find that

$$(M + M_x\delta x) - M + (Q + Q_x\delta x)\delta x + \Delta p\frac{(\delta x)^2}{2} = 0$$

which, in the limit as δx tends to zero, becomes

$$M_x + Q = 0. \tag{7}$$

If we now combine (6) and (7) with $M = \gamma S_{xx}$ (which relates bending moment and curvature) we find that (in non-dimensional variables, with $p = \epsilon\rho U_\infty^2 p^*$ since we expect the pressure difference across the flag to be $O(\epsilon\rho U_\infty^2)$)

$$-\frac{\gamma\epsilon}{L^3\rho U_\infty^2} S^*_{x^*x^*x^*x^*} + \epsilon\Delta p^* = \frac{\epsilon\rho'}{L\rho} S^*_{t^*t^*}. \tag{8}$$

We note that (8) includes no $S^*_{x^*x^*}$ term; such a term could be added, however, to model the effects of shear stress due to the free-stream flow. The coefficient multiplying this term would vary according to whether one wished to account for laminar drag, turbulence effects, vortices that might be shed from the flagpole, or other effects. Since we wish to introduce as few

unknown effects as possible into the model, we do not proceed further with such modelling here.

The quantity Δp^* is found by applying the unsteady Bernoulli equation in the limit as y tends to zero. We have

$$[\phi_t]_{0^-}^{0^+} + \frac{1}{\rho}[p]_{0^-}^{0^+} + \frac{1}{2}[\psi_y^2 + \psi_x^2]_{0^-}^{0^+} = 0. \tag{9}$$

As in other studies, (see, for example [4], [5] and many others), we assume that the first term in (9) may be ignored. This is tantamount to assuming that the vorticity shed from the flag does not influence the flag itself. Though it seems to have become normal to proceed under this assumption, inclusion of this term, which amounts to an integral of $-f_{t^*}^*$ between 0 and x^*, would not actually change the model very much. The function f^* would obey a simple integral equation involving S^* and its derivatives, which would have to be solved in conjunction with (5). The methods developed below could be used with a few small changes to accomplish this. We do not pursue this matter further in the current study, however.

When we use our previous expressions (4) for the derivatives of ψ, we find that

$$\epsilon U_\infty^2 (p_+^* - p_-^*) + \frac{U_\infty^2}{2}\left[\left(1 + \frac{\epsilon}{2}f^*\right)^2 - \left(1 - \frac{\epsilon}{2}f^*\right)^2\right] + O(\epsilon^2) = 0$$

and thus

$$f^* = p_-^* - p_+^*$$

across the flag, and is zero otherwise. When this is combined with (8), we find that, across the flag,

$$-\frac{\gamma}{\rho L^3 U_\infty^2} S^*_{x^*x^*x^*x^*} + f^* = \frac{\rho'}{L\rho} S^*_{t^*t^*},$$

which, when substituted in (5), gives

$$S^*_{t^*} + S^*_{x^*}\left(1 + \frac{\epsilon}{2}\left(\frac{\rho'}{L\rho}S^*_{t^*t^*} + \frac{\gamma}{\rho L^3 U_\infty^2} S^*_{x^*x^*x^*x^*}\right)\right) =$$

$$\alpha^*(t^*) - \frac{1}{2\pi}\int_0^{c/L} \frac{\dfrac{\rho'}{L\rho}S^*_{t^*t^*} + \dfrac{\gamma}{\rho L^3 U_\infty^2} S^*_{\eta^*\eta^*\eta^*\eta^*}}{x^* - \eta^*} \mathrm{d}\eta^*.$$

Ostensibly, the upper limit of the singular integral in this equation is an unknown quantity that depends upon the shape of the flag. However, the (dimensional) flag length condition is evidently

$$L = \int_0^c \sqrt{1 + S_x^2}\,\mathrm{d}x,$$

which, in non-dimensional variables, becomes

$$L - c = \frac{L}{2}\epsilon^2 \int_0^{\frac{c}{L}} {S^*_{x^*}}^2 \mathrm{d}x^* + o(\epsilon^2).$$

Thus, for $O(\epsilon)$ perturbations of the flag, the trailing edge moves horizontally by only $O(\epsilon^2)$, so that to leading order $L = c$. The final leading-order equation for unsteady flag motion is therefore

$$\mu^*(S^*_{t^*} + S^*_{x^*} - \alpha^*) = \frac{1}{\pi} \int_0^1 \frac{S^*_{t^*t^*} + \gamma^* S^*_{\eta^*\eta^*\eta^*\eta^*}}{\eta^* - x^*} \mathrm{d}\eta^*, \tag{10}$$

where μ^* and γ^*, the two key non-dimensional parameters in the problem, are defined by

$$\mu^* = \frac{2\rho L}{\rho'}, \qquad \gamma^* = \frac{\gamma}{\rho' L^2 U_\infty^2}.$$

μ^* may be thought of as measuring the fluid/flag density ratio; γ^* determines the relative importance of flag rigidity and momentum flux.

We must now consider the specification of boundary and initial conditions for this equation.

2.1. Boundary and initial conditions

We consider both clamped and hinged flags. For a flag clamped with zero slope at its leading edge, we have $S^*(0, t^*) = 0$ and $S^*_{x^*}(0, t^*) = 0$, whilst for a hinged flag the bending moment at the leading edge is zero so that $S^*(0, t^*) = 0$ and $S^*_{x^*x^*}(0, t^*) = 0$.

The boundary conditions at the free end of the flag are the same for both the clamped and hinged cases. Since the trailing edge is free, the shearing force is zero at $x^* = 1$ and the non-dimensional version of Equation (7) therefore implies that $M_{x^*}(1, t^*) = 0$ and so $S^*_{x^*x^*x^*}(1, t^*) = 0$. The bending moment is also zero at the trailing edge and hence $S^*_{x^*x^*}(1, t^*) = 0$. Finally, we impose a Kutta condition. This amounts to the fact that the vortex strength at the flag trailing edge must be zero. Thus

$$S^*_{t^*t^*}(1, t^*) + \gamma^* S^*_{x^*x^*x^*x^*}(1, t^*) = 0. \tag{11}$$

It is worth pointing out that opinion is by no means unanimous (see, for example [8]) that the Kutta condition is the correct one to impose for an unsteady flow past a deforming object. We do so in this study, however, since we take the view that discontinuous pressures must be avoided. One possible interpretation of the inviscid incompressible limit considered in [8] is that it may be impossible to avoid pressure jumps at the trailing edge. If a Kutta condition was not imposed then then the consequences for the stability of the flag may be severe. Further investigation of the validity of this limit is clearly required (though is beyond the scope of this paper).

As far as initial conditions are concerned, since the equation is second-order in time, we specify $S^*(x^*, 0)$ and $S^*_{t^*}(x^*, 0)$; for the remainder of this study we consider flags that are initially stationary so that $S^*_{t^*}(x^*, 0) = 0$.

3. The steady flag

Before analysing the full unsteady flag equation it is illuminating to first examine the steady problem where α^* is time-independent. When all time derivatives are set equal to zero in (10), we obtain

$$\kappa^*(S^{*\prime} - \alpha^*) = \frac{1}{\pi} \int_0^1 \frac{S^{*\prime\prime\prime\prime}(\eta^*)}{\eta^* - x^*} \mathrm{d}\eta^*, \tag{12}$$

the boundary conditions being $S^*(0) = S^{*\prime\prime}(1) = S^{*\prime\prime\prime}(1) = 0$ along with the Kutta condition $S^{*\prime\prime\prime\prime}(1) = 0$ and either $S^{*\prime}(0) = 0$ (clamped flag) or $S^{*\prime\prime}(0) = 0$ (hinged flag). The Equation (12) is somewhat similar to the equation governing the deflection of steady sails that was first proposed by Voelz in [9] and later studied in detail by Thwaites in [10]; however, the 'sail' equation is second order only. The steady flag equation (12) contains a single non-dimensional parameter κ^*, defined by

$$\kappa^* = \frac{\mu^*}{\gamma^*} = \frac{2\rho L^3 U_\infty^2}{\gamma}.$$

The parameter κ^* therefore characterises the ratio of the free stream momentum to the flexural rigidity of the flag (and is independent of the mass of the flag, ρ', a logical result since evidently a change in flag mass does not affect the steady solution). For small values of κ^* the flag is so stiff that the outer flow is unable to materially influence its shape for the small angles of incidence under consideration. This case is examined in the next section. In the limit as κ^* tends to infinity the flexural rigidity of the flag is negligible compared to the outer flow momentum, and equation (12) reduces to $S^{*\prime}(x^*) = \alpha^*$. For a hinged flag the solution is clearly $S^* = \alpha^* x^*$. For a clamped flag a little more care is required; away from $x^* = 0$ the outer solution is still $S^* = \alpha^* x^*$, but the boundary condition $S^{*\prime}(0) = 0$ is satisfied by introducing a boundary layer of width $\kappa^{-1/3}$ near to $x^* = 0$ (a result that has striking similarities to the boundary layers that are commonly encountered in the theory of the 'stiffened catenary').

3.1. The limit of large flexural rigidity

In the limit $\kappa^* \to 0$ with $\alpha^* = O(1)$, (a very 'stiff' flag) Equation (12) becomes (upon inversion and imposition of the Kutta condition) (see, for example [11, Chapter 6])

$$S^{*\prime\prime\prime\prime}(x^*) = 0.$$

The solution for a hinged flag is therefore $S^*(x^*) = \alpha^* x^*$, so that the flag simply aligns with the outer flow. For a clamped flag, we find that $S^*(x^*) = 0$, which amounts to the fact that the outer flow is insufficiently strong to affect the flag curvature.

A more interesting limit arises when $\kappa^* \to 0$ but $\kappa^*\alpha^*$ is of order one (so that the angle of incidence, whilst still remaining small, is an order of magnitude larger). For the hinged case, $S^{*\prime} = O(\alpha^*)$ and the flag still aligns with the flow. For the clamped flag S^* is $O(1)$ and (12) becomes

$$\frac{1}{\pi} \int_0^1 \frac{S^{*\prime\prime\prime\prime}}{\eta^* - x^*} \mathrm{d}\eta^* = -\kappa^*\alpha^*.$$

The solution for the clamped case may now be obtained by inverting the above equation and imposing the Kutta condition to give

$$S^{*\prime\prime\prime\prime}(x^*) = \kappa^*\alpha^* \sqrt{\frac{1 - x^*}{x^*}}.$$

We may now integrate four times with respect to x^* and apply the boundary conditions to yield

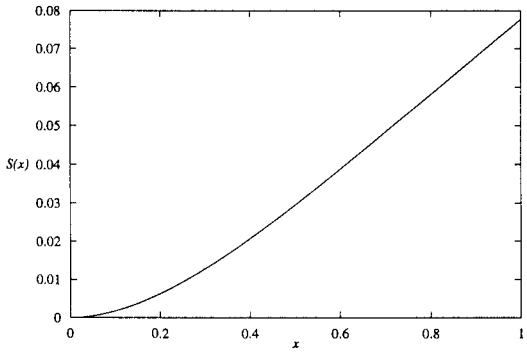

Figure 3. The clamped flag of large flexural rigidity.

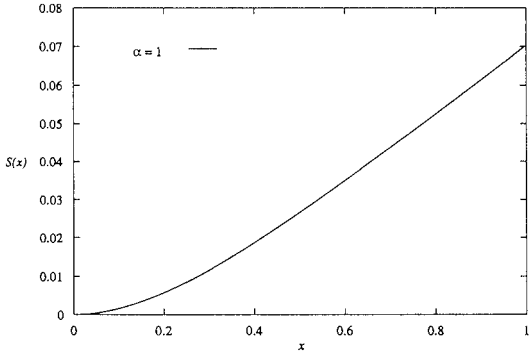

Figure 4. Clamped flag with $\kappa = 1$, $\alpha = 1$.

$$S^*(x^*) = \kappa^*\alpha^*\left[\left(\frac{x^{*3}}{24} + \frac{13x^{*2}}{144} - \frac{31x^*}{576} + \frac{5}{384}\right)\sqrt{x^*}\sqrt{1-x^*} + \left(\frac{x^{*3}}{12} - \frac{x^{*2}}{16} + \frac{x^*}{32} - \frac{5}{768}\right)\arcsin(2x^* - 1) - \frac{\pi}{24}x^{*3} + \frac{\pi}{32}x^{*2} + \frac{\pi}{64}x^* - \frac{5\pi}{1536}\right].$$

The flag shape for $\kappa^*\alpha^* = 1$ is presented in Figure 3; as might be expected for a clamped, stiff flag the non-dimensional deviations in flag position are small.

3.2. Numerical procedure for solution of the steady flag equation

When the full steady flag equation (12) applies, it is necessary to proceed numerically. The first step is to invert (12). The theory of singular integral equations (see, for example, [11]) asserts that the solution to

$$-\frac{1}{\pi}\int_a^b \frac{\phi(\eta)}{\eta - x}\mathrm{d}\eta = g(x)$$

is given by any one of

$$\frac{1}{\pi}\sqrt{\frac{b-x}{x-a}}\int_a^b \sqrt{\frac{\eta-a}{b-\eta}}\frac{g(\eta)}{\eta - x}\mathrm{d}\eta + \frac{C}{\sqrt{(b-x)(x-a)}}, \tag{13}$$

$$\frac{1}{\pi}\sqrt{\frac{x-a}{b-x}}\int_a^b \sqrt{\frac{b-\eta}{\eta-a}}\frac{g(\eta)}{\eta - x}\mathrm{d}\eta + \frac{C'}{\sqrt{(b-x)(x-a)}}, \tag{14}$$

$$\frac{1}{\pi}\int_a^b \sqrt{\frac{(b-\eta)(\eta-a)}{(b-x)(x-a)}}\frac{g(\eta)}{\eta - x}\mathrm{d}\eta + \frac{C''}{\sqrt{(b-x)(x-a)}}, \tag{15}$$

where C, C' or C'' are suitably-chosen eigenconstants and the choice of which of (13–15) to use is determined by the desired finiteness properties of the solution at $x = a$ and $x = b$. In

our case applying the Kutta condition is tantamount to using (13) and choosing C suitably, whence we obtain

$$S''''(x) = -\frac{\kappa}{\pi}\sqrt{\frac{1-x}{x}}\int_0^1 \sqrt{\frac{\eta}{1-\eta}}\left(\frac{S'}{\eta - x}\right)\mathrm{d}\eta + \kappa\alpha\sqrt{\frac{1-x}{x}}. \tag{16}$$

(Here and henceforth the stars are omitted for clarity.) It is worth noting at this stage that many valuable simplifications are possible if the steady equation (16) is manipulated using the well-known Glauert transformation and series (see, for example [12, Chapter 8]). We do not proceed further along such lines, however, since our main objective is to develop methods which may easily be generalised to the full unsteady problem.

To formulate a finite-difference method for (16), the region $0 \le x \le 1$ is divided into n equally spaced intervals. The $n+1$ mesh points are denoted by $\eta_i = i\delta x$ (with $\delta x = 1/n$) for $i = 0, 1, \ldots, n$ and the approximation to $S(\eta_i)$ is henceforth denoted by S_i. The $S''''(x)$ term is discretised using the central-difference formula

$$S''''(\eta_i) \approx \frac{1}{(\delta x)^4}(S_{i+2} - 4S_{i+1} + 6S_i - 4S_{i-1} + S_{i-2}). \tag{17}$$

To discretise the singular integral term in (16), we express the integral as a sum of integrals over each sub-interval $[\eta_{i-1}, \eta_i]$, so that

$$\begin{aligned} I &= -\frac{\kappa}{\pi}\sqrt{\frac{1-x}{x}}\int_0^1 \sqrt{\frac{\eta}{1-\eta}}\frac{S'(\eta)}{(\eta - x)}\mathrm{d}\eta \\ &= -\frac{\kappa}{\pi}\sqrt{\frac{1-x}{x}}\sum_{k=1}^{n}\int_{\eta_{k-1}}^{\eta_k} \sqrt{\frac{\eta}{1-\eta}}\frac{S'(\eta)}{(\eta - x)}\mathrm{d}\eta. \end{aligned} \tag{18}$$

We now assume that S' is piecewise constant on the interval $[\eta_{k-1}, \eta_k]$ and is equal to $(S'(\eta_{k-1}) + S'(\eta_k))/2$. Hence (18) becomes

$$I \approx -\frac{\kappa}{2}\sum_{k=1}^{n}\big(S'(\eta_{k-1}) + S'(\eta_k)\big)\left[\frac{1}{\pi}\sqrt{\frac{1-x}{x}}\int_{\eta_{k-1}}^{\eta_k}\sqrt{\frac{\eta}{1-\eta}}\frac{\mathrm{d}\eta}{(\eta - x)}\right].$$

If we now evaluate the integral, we find that

$$\begin{aligned} I \approx\ & -\frac{\kappa}{2}\sum_{k=1}^{n}\big(S'(\eta_{k-1}) + S'(\eta_k)\big) \times \\ & \left[\frac{2}{\pi}\sqrt{\frac{1-x}{x}}\arcsin(\sqrt{\eta}) + \frac{1}{\pi}\log\left|\frac{\sqrt{\frac{\eta}{1-\eta}} - \sqrt{\frac{x}{1-x}}}{\sqrt{\frac{\eta}{1-\eta}} + \sqrt{\frac{x}{1-x}}}\right|\right]_{\eta=\eta_{k-1}}^{\eta=\eta_k}. \end{aligned} \tag{19}$$

Care must be exercised in choosing the collocation points since the logarithmic term in equation (19) is unbounded when $x = \eta$. We therefore collocate at the mid-point of each sub-interval to give

$$I \approx -\kappa\sum_{k=1}^{n} Q_{ik}(S'(\eta_{k-1}) + S'(\eta_k)), \tag{20}$$

where Q_{ik} is given by

$$Q_{ik} = \frac{1}{\pi}\sqrt{\frac{2(n-i)+1}{2i-1}}\left\{\arcsin\left(\sqrt{\frac{k}{n}}\right) - \arcsin\left(\sqrt{\frac{k-1}{n}}\right)\right\} + \\ + \frac{1}{2\pi}\log\left|\frac{\sqrt{2(k-1)(n-i)+k-1}+\sqrt{(2i-1)(n-k+1)}}{\sqrt{2(k-1)(n-i)+k-1}-\sqrt{(2i-1)(n-k+1)}}\,\frac{\sqrt{2k(n-i)+k}+\sqrt{(2i-1)(n-k)}}{\sqrt{2k(n-i)+k}-\sqrt{(2i-1)(n-k)}}\right|. \tag{21}$$

Forward differences are used to discretise the first order derivatives of S, except for $S'(\eta_n)$ for which backward differences are used since the point η_{n+1} is undefined. Hence equation (20) becomes

$$I \approx -\frac{\kappa}{\delta x}\sum_{k=1}^{n-1} Q_{ik}(S_{k+1}-S_{k-1}) - \frac{2\kappa Q_{in}}{\delta x}(S_n - S_{n-1}).$$

The discrete problem (which is to be solved for $i = 1, 2, ..., n$) is therefore

$$(S_{i+2} - 4S_{i+1} + 6S_i - 4S_{i-1} + S_{i-2}) + \kappa(\delta x)^3\sum_{k=1}^{n-1} Q_{ik}(S_{k+1}-S_{k-1}) + \\ + 2\kappa Q_{in}(\delta x)^3(S_n - S_{n-1}) = \kappa\alpha(\delta x)^4\sqrt{\frac{n-i}{i}}.$$

The boundary conditions must now be used to eliminate the fictitious mesh points. This may be done in the normal way to yield the equations

$$(S_3 - 4S_2 + MS_1) + \kappa(\delta x)^3\sum_{k=1}^{n-1} Q_{1k}(S_{k+1}-S_{k-1}) + \\ + 2\kappa Q_{1n}(\delta x)^3(S_n - S_{n-1}) = \kappa\alpha(\delta x)^4\sqrt{n-1}, \tag{22}$$

$$(S_{i+2} - 4S_{i+1} + 6S_i - 4S_{i-1} + S_{i-2}) + \kappa(\delta x)^3\sum_{k=1}^{n-1} Q_{ik}(S_{k+1}-S_{k-1}) + \\ + 2\kappa Q_{in}(\delta x)^3(S_n - S_{n-1}) = \kappa\alpha(\delta x)^4\sqrt{\frac{n-i}{i}} \quad (i = 2, 3, \ldots, n-2), \tag{23}$$

$$(-2S_n + 5S_{n-1} - 4S_{n-2} + S_{n-3}) + \kappa(\delta x)^3\sum_{k=1}^{n-1} Q_{n-1,k}(S_{k+1}-S_{k-1}) + \\ + 2\kappa Q_{n-1,n}(\delta x)^3(S_n - S_{n-1}) = \frac{\kappa\alpha(\delta x)^4}{\sqrt{n-1}}, \tag{24}$$

$$(S_n - 2S_{n-1} + S_{n-2}) + \kappa(\delta x)^3\sum_{k=1}^{n-1} Q_{nk}(S_{k+1}-S_{k-1}) + \\ + 2\kappa Q_{nn}(\delta x)^3(S_n - S_{n-1}) = 0, \tag{25}$$

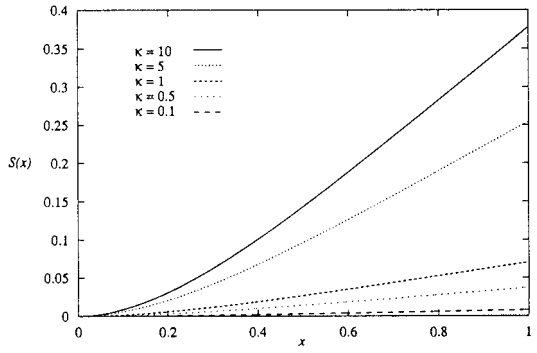

*Figure 5.*Clamped flags for $\alpha = 1$.

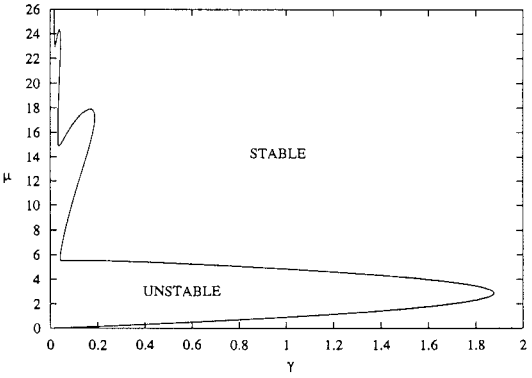

Figure 6. Marginal stability plot for the hinged flag.

where $M = 5$ for the hinged flag and $M = 7$ for the clamped flag. The linear system (22–25) may be solved using a standard library routine (the NAG routine F04ATF was used in this instance and coding was carried out in FORTRAN-77 on a SUN SPARC2).

3.2.1. *Numerical solutions of the steady flag equation*
Tests showed that as n increased successive solutions became ever closer; the results presented here are calculated with $n = 500$. As expected, steady solutions for the hinged flag all align with the outer flow and agree with the exact solution $S = \alpha x$.

The clamped flag, however, cannot align with the outer flow for non-zero α. Figure 4 shows results obtained for a clamped flag with $\kappa = 1$ and $\alpha = 1$. The clamping has a significant effect on the flag shape when compared to the hinged flag results. However, this deviation (which, from (16), obviously depends in a linear fashion on α) is far less than in the hinged case; for example, the results for $\alpha = 1$ indicate that $S(1) \approx 0{\cdot}07$ for the clamped flag compared to $S(1) = 1$ for the corresponding hinged case.

Results for different values of κ are shown in Figure 5 and are equally predictable; as κ decreases the flag becomes stiffer and is less able to bend.

4. Linear stability analysis of the unsteady flag equation

In order to determine whether or not steady solutions of (10) might ever be observed in practice, it is necessary to determine if they are stable. In this section we therefore examine the linear stability of steady solutions. As usual, we assume a perturbation of the form

$$S(x, t) = \overline{S}(x) + f(x)\mathrm{e}^{\sigma t}, \tag{26}$$

where $f(x)$ is 'small' and $\overline{S}$ is a steady solution. The linearity of the governing equation means that neither $\overline{S}$ nor α appear in the linear stability problem; stability is thus determined only by the values of γ and μ. The analysis is complicated by the fact that an exponential *Ansatz* for $f(x)$ is not possible since the finite-range Hilbert transform of an exponential is not an exponential.

We begin by inverting the unsteady flag equation (10) and imposing the Kutta condition to give

$$S_{tt} + \gamma S_{xxxx} + \frac{\mu}{\pi}\sqrt{\frac{1-x}{x}} \int_0^1 \sqrt{\frac{\eta}{1-\eta}} \left(\frac{S_t + S_\eta}{\eta - x} \right) \mathrm{d}\eta = \mu\alpha(t)\sqrt{\frac{1-x}{x}}. \tag{27}$$

When (27) is perturbed using (26), we find that

$$\begin{aligned} \sigma^2 f \; + \; \sigma \left[\frac{\mu}{\pi}\sqrt{\frac{1-x}{x}} \int_0^1 \sqrt{\frac{\eta}{1-\eta}} \frac{f(\eta)}{(\eta - x)} \mathrm{d}\eta \right] + \\ + \gamma f'''' + \frac{\mu}{\pi}\sqrt{\frac{1-x}{x}} \int_0^1 \sqrt{\frac{\eta}{1-\eta}} \frac{f'(\eta)}{(\eta - x)} \mathrm{d}\eta = 0. \end{aligned} \tag{28}$$

The boundary conditions are $f(0) = f''(1) = f'''(1) = 0$ along with $f''(0) = 0$ for the hinged flag and $f'(0) = 0$ for the clamped flag; as usual, we seek to determine values of σ, γ and μ for which (28) has a non-zero solution.

The region $0 \le x \le 1$ is again divided into n equally spaced intervals, the mesh-points of which are denoted by $\eta_i = in^{-1}$ for $i = 0, 1, \ldots, n$. The fourth derivative of f is discretised using the finite-difference approximation (17) leaving the task of discretising the singular integrals. Since both $f(\eta)$ and $f'(\eta)$ are present in Equation (28), we assume that $f(\eta)$ is piecewise linear over each interval, and thus

$$f'(\eta) \approx \frac{f_i - f_{i-1}}{\eta_i - \eta_{i-1}} = \frac{1}{\delta x}(f_i - f_{i-1})$$

and so for $\eta \in [\eta_{i-1}, \eta_i]$

$$f(\eta) \approx \frac{1}{\delta x}(f_i - f_{i-1})(\eta - \eta_{i-1}) + f_{i-1}.$$

The singular integral involving $f'(\eta)$ in equation (28) is discretised by means of the method detailed in Section 3.2 to give

$$I = \frac{\mu}{\pi}\sqrt{\frac{1-x}{x}} \int_0^1 \sqrt{\frac{\eta}{1-\eta}} \frac{f'(\eta)}{(\eta - x)} \mathrm{d}\eta \approx \frac{2\mu}{\delta x} \sum_{k=1}^{n} Q_{ik}(f_k - f_{k-1}),$$

where Q_{ik} is given by (21). To discretise the other integral in (28) we use

$$\begin{aligned} J \; &= \; \frac{\mu}{\pi}\sqrt{\frac{1-x}{x}} \int_0^1 \sqrt{\frac{\eta}{1-\eta}} \frac{f(\eta)}{(\eta - x)} \mathrm{d}\eta \\ &\approx \; \frac{\mu}{\pi}\sqrt{\frac{1-x}{x}} \sum_{k=1}^{n} \int_{\eta_{k-1}}^{\eta_k} \sqrt{\frac{\eta}{1-\eta}} \left[\frac{1}{\delta x}(f_k - f_{k-1})(\eta - \eta_{k-1}) + f_{k-1} \right] \frac{\mathrm{d}\eta}{(\eta - x)}, \end{aligned}$$

so that

$$\begin{aligned} J \; \approx \; & \frac{\mu}{\delta x} \sum_{k=1}^{n} (f_k - f_{k-1}) \left[\frac{1}{\pi}\sqrt{\frac{1-x}{x}} \int_{\eta_{k-1}}^{\eta_k} \frac{\eta^{\frac{3}{2}}}{\sqrt{1-\eta}} \frac{\mathrm{d}\eta}{(\eta - x)} \right] - \\ & - 2\mu \sum_{k=1}^{n} (k-1) Q_{ik}(f_k - f_{k-1}) + 2\mu \sum_{k=1}^{n} Q_{ik} f_{k-1}. \end{aligned}$$

We now evaluate

$$R(x,\eta)=\frac{1}{\pi}\sqrt{\frac{1-x}{x}}\int_{\eta_{k-1}}^{\eta_k}\frac{\eta^{\frac{3}{2}}}{\sqrt{1-\eta}}\frac{\mathrm{d}\eta}{(\eta-x)}$$

using standard integrals and set $\eta_k=kn^{-1}$ and $x_i=(2i-1)/2n$ to give

$$\begin{aligned}R_{ik} \;=\; & \frac{1}{2\pi}\sqrt{\frac{2(n-i)+1}{2i-1}}\left\{\arcsin\left(\frac{2k-n}{n}\right)-\arcsin\left(\frac{2k-2-n}{n}\right)-\right.\\ & \left.-\frac{2}{n}\sqrt{k(n-k)}+\frac{2}{n}\sqrt{(k-1)(n-k+1)}\right\}+\frac{(2i-1)Q_{ik}}{n}. \qquad (29)\end{aligned}$$

The discretisation of the perturbed equation (28) is thus

$$\begin{aligned}&\sigma^2 f_i+\sigma\left[\sum_{k=1}^{n}\left\{\frac{\mu}{\delta x}R_{ik}(f_k-f_{k-1})-2\mu(k-1)Q_{ik}(f_k-f_{k-1})+2\mu Q_{ik}f_{k-1}\right\}\right]+\\ &\quad+\left[\frac{\gamma}{(\delta x)^4}(f_{i+2}-4f_{i+1}+6f_i-4f_{i-1}+f_{i-2})+\frac{2\mu}{\delta x}\sum_{k=1}^{n}Q_{ik}(f_k-f_{k-1})\right]=0 \qquad (30)\end{aligned}$$

for $i=1,2,\ldots,n$ where Q_{ik} is given by (21) and R_{ik} by (29). The boundary conditions are again used to eliminate the fictitious mesh points in (30). The full numerical problem is thus given by

$$\begin{aligned}&\sigma^2 f_1 \;+\; \sigma\left[\sum_{k=1}^{n}\left\{\frac{\mu}{\delta x}R_{1k}(f_k-f_{k-1})-2\mu(k-1)Q_{1k}(f_k-f_{k-1})+2\mu Q_{1k}f_{k-1}\right\}\right]+\\ &\quad+\left[\frac{\gamma}{(\delta x)^4}(f_3-4f_2+Mf_1)+\frac{2\mu}{\delta x}\sum_{k=1}^{n}Q_{1k}(f_k-f_{k-1})\right]=0, \qquad (31)\end{aligned}$$

$$\begin{aligned}&\sigma^2 f_i \;+\; \sigma\left[\sum_{k=1}^{n}\left\{\frac{\mu}{\delta x}R_{ik}(f_k-f_{k-1})-2\mu(k-1)Q_{ik}(f_k-f_{k-1})+2\mu Q_{ik}f_{k-1}\right\}\right]+\\ &\quad+\left[\frac{\gamma}{(\delta x)^4}(f_{i+2}-4f_{i+1}+6f_i-4f_{i-1}+f_{i-2})+\frac{2\mu}{\delta x}\sum_{k=1}^{n}Q_{ik}(f_k-f_{k-1})\right]=0,\\ &\quad(i=2,3,..n-2), \qquad (32)\end{aligned}$$

$$\begin{aligned}&\sigma^2 f_{n-1}+\sigma\left[\sum_{k=1}^{n}\left\{\frac{\mu}{\delta x}R_{n-1,k}(f_k-f_{k-1})-\right.\right.\\ &\quad\left.\left.-\;2\mu(k-1)Q_{n-1,k}(f_k-f_{k-1})+2\mu Q_{n-1,k}f_{k-1}\right\}\right]+\\ &\quad+\left[\frac{\gamma}{(\delta x)^4}(-2f_n+5f_{n-1}-4f_{n-2}+f_{n-3})+\frac{2\mu}{\delta x}\sum_{k=1}^{n}Q_{n-1,k}(f_k-f_{k-1})\right]\\ &\quad=0, \qquad (33)\end{aligned}$$

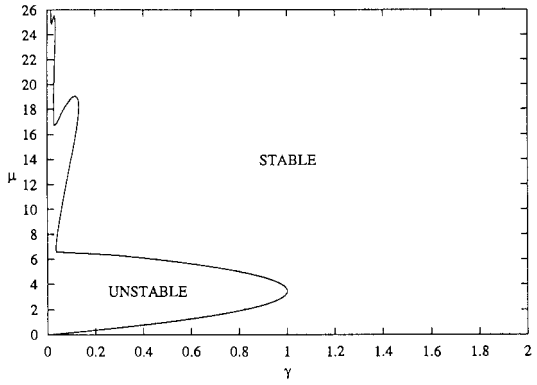

Figure 7. Marginal stability plot for the clamped flag.

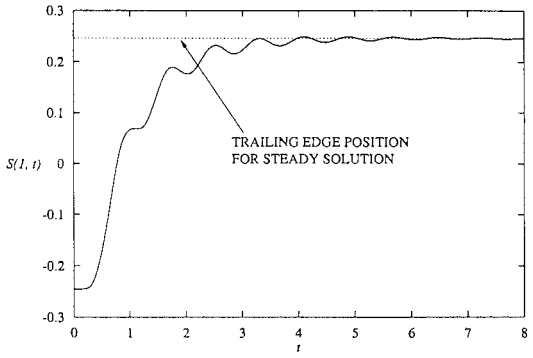

Figure 8. $S(1, t)$ for the hinged flag With $\gamma = 0{\cdot}2$ and $\mu = 7$.

and

$$\sigma^2 f_n + \sigma\left[\sum_{k=1}^{n}\left\{\frac{\mu}{\delta x}R_{nk}(f_k - f_{k-1}) - 2\mu(k-1)Q_{nk}(f_k - f_{k-1}) + 2\mu Q_{nk} f_{k-1}\right\}\right] + \left[\frac{\gamma}{(\delta x)^4}(f_n - 2f_{n-1} + f_{n-2}) + \frac{2\mu}{\delta x}\sum_{k=1}^{n} Q_{nk}(f_k - f_{k-1})\right] = 0, \tag{34}$$

where $M = 5$ for the hinged flag and $M = 7$ for the clamped flag.

The Equations (31–34) are a system of n homogeneous equations for the n unknowns $f_1, \ldots, f_n$. Introduction of the vector $\underline{f} = (f_1, f_2, ..., f_n)^T$ enables the problem to be written in matrix form to give the quadratic eigenvalue problem

$$\sigma^2 \mathbf{I}\underline{f} + \sigma\mathbf{A}\underline{f} + \mathbf{B}\underline{f} = \underline{0}.$$

We may simplify this by introducing the vector $\underline{f}^* = \sigma\underline{f}$ to give the standard eigenvalue problem

$$\mathbf{M}\underline{g} = \sigma\underline{g}, \tag{35}$$

where $\underline{g} = (\underline{f}, \underline{f}^*)^T$ and

$$\mathbf{M} = \begin{pmatrix} \mathbf{0} & \mathbf{I} \\ -\mathbf{B} & -\mathbf{A} \end{pmatrix}.$$

We may solve the eigenvalue problem (35) for a given γ, μ and n using the NAG routine F02EBF and the $2n$ eigenvalues analysed to locate the eigenvalue with $\max(\mathfrak{Re}(\sigma))$. As usual, a positive value of $\max(\mathfrak{Re}(\sigma))$ implies instability.

Marginal stability curves for hinged and clamped flags are presented in Figure 6 and Figure 7, respectively. (It is worth noting that, though we have chosen to use γ and μ as axes, in some branches of the aeroelastic literature it has become traditional to plot μ *vs.* μ/γ.)

For $\gamma > 1{\cdot}88$ the hinged flag is stable regardless of the mass of the flag. Sufficiently stiff flags are therefore always stable. For a clamped flag similar behaviour is present, though

for guaranteed stability we now only require $\gamma > 0{\cdot}99$. This smaller value of γ reflects the physically obvious fact that a hinged flag is able to move without changing its curvature, whilst a clamped flag does not enjoy the freedom of a pivoted leading edge.

For smaller values of γ, the motion may be stable or unstable depending on the value of μ; the qualitative shapes of the marginal stability curves are similar for both clamped and hinged flags. When γ is very small, the motion is always unstable, as expected. For a fixed value of γ of approximately $0{\cdot}1$ as μ increases from 0 (a very heavy flag) a small region of stability is present before instability sets in. The instability typically manifests itself as a first-order mode solution where a point near to the centre of the flag remains virtually stationary (see later). As μ increases further another region of stability is encountered before second-mode instabilities appear.

The limit $\mu \to 0$ may be investigated without the need for numerical calculations; unsurprisingly, however, the analysis, which is of a standard nature, simply reveals that an infinitely heavy flag is neutrally stable as the outer flow is unable to move it. For full details, see [13].

5. The unsteady flag

We now turn our attention to the full unsteady problem (10). Very little literature seems previously to have appeared that concerns itself with the numerical solution of partial singular integro-differential equations with Cauchy kernel. This is a little surprising, since such equations arise in a number of different branches of applied mathematics (see, for example the discussion of the Benjamin-Ono equation in [9] and [10]). One reason for this may be that difficulties arise in dealing with the Cauchy kernel. Since no standard methods for such equations seem to exist, we proceed in an *ad hoc* fashion by designing an explicit numerical scheme that relies on inversion of the equation. We prove only limited results concerning the numerical stability of the method, though many numerical experiments convinced us that the proposed scheme was accurate and stable.

Our reasons for wishing to compute numerical solutions to the full unsteady problem are twofold; first, we wish to have some means of verifying the predictions of the linear stability analysis presented in the last section, and, second, we wish to be able to track the shape of the flag over time as the angle of incidence changes in a general fashion.

Before considering numerical methods for the full unsteady equation, we note that there are a few limiting cases where some analytical progress may be made. In the limit $\gamma \to 0$ (a flag with no stiffness) the problem reduces to the equation studied in [2]. It is easy to show, however, that all motions of such flags are unstable. We therefore examine the limit $\gamma \to \infty$ in the next section.

5.1. The large flexural rigidity limit

In the limit as $\gamma \to \infty$ but $\mu\alpha$ is of order one (10) becomes

$$S_{xxxx}(x, t) = 0. \tag{36}$$

For a hinged flag, the solution to (36) is $S(x, t) = \alpha(t)x$. A hinged flag therefore aligns itself instantaneously with the flow for all $\alpha(t)$. For a clamped flag, however, the solution is simply $S(x, t) = 0$. In this case the flag is too stiff to be influenced by the outer flow.

A more interesting limit arises when $\gamma \to \infty$ but $\mu\alpha\gamma^{-1}$ is of order one. For a clamped flag, (10) reduces to the quasi-steady equation

$$\frac{1}{\pi}\fint_0^1 \frac{S_{\eta\eta\eta\eta}}{\eta - x}\mathrm{d}\eta = -\frac{\mu\alpha(t)}{\gamma}. \tag{37}$$

The Kutta condition (11) becomes $S_{xxxx}(1,t) = 0$ in the limit as $\gamma \to \infty$ and (37) may be inverted and solved analytically (subject to the boundary conditions $S(0,t) = S_x(0,t) = S_{xx}(1,t) = S_{xxx}(1,t) = 0$) to yield the quasi-steady solution

$$S(x,t) = \frac{\mu\alpha(t)}{\gamma}\left[\left(\frac{x^3}{24} + \frac{13x^2}{144} - \frac{31x}{576} + \frac{5}{384}\right)\sqrt{x}\sqrt{1-x} + \right.$$
$$\left. + \left(\frac{x^3}{12} - \frac{x^2}{16} + \frac{x}{32} - \frac{5}{768}\right)\arcsin(2x-1) - \frac{\pi}{24}x^3 + \frac{\pi}{32}x^2 + \frac{\pi}{64}x - \frac{5\pi}{1536}\right].$$

If we try to repeat this process for a hinged flag with $S(0,t) = S_{xx}(0,t) = S_{xx}(1,t) = S_{xxx}(1,t) = 0$, we find that there is no solution. This is because S is no longer $O(1)$ for a hinged flag. Two sub-cases must now be considered; when $\mu = O(1)$ and $\alpha \to \infty$ with $\alpha/\gamma = O(1)$, it transpires that $S = O(\alpha)$, the leading-order equation is $S_{xxxx}(x,t) = 0$, and therefore $S(x,t) = \alpha(t)x$. When $\alpha = O(1)$ and $\mu \to \infty$ with $\mu/\gamma = O(1)$, S is once again $O(1)$ but now satisfies

$$\frac{\mu}{\gamma}(S_t + S_x - \alpha) = \frac{1}{\pi}\fint_0^1 \frac{S_{\eta\eta\eta\eta}}{\eta - x}\mathrm{d}\eta.$$

This equation could be solved using an explicit scheme but we do not pursue the matter further here.

5.2. Discretisation of the unsteady flag equation

Now that we have considered some limiting cases, we turn to the general numerical solution of the unsteady flag equation. Our basic method is to employ an explicit finite difference scheme on the inverted unsteady flag equation (27). The region $0 \le x \le 1$ is again divided into n equally spaced intervals. We use the method of Section 3.2 to discretise the singular integral in (27), central differences for the fourth derivative term, an explicit central difference for the S_{tt} term, and, in order to produce an explicit scheme, we employ a backward difference for the S_t term. This gives (for $i = 0, 1, ..., n$ and $j = 0, 1, ...$)

$$\begin{aligned} S_i^{j+1} \;=\; & 2S_i^j - S_i^{j-1} - \frac{\gamma(\delta t)^2}{(\delta x)^4}(S_{i+2}^j - 4S_{i+1}^j + 6S_i^j - 4S_{i-1}^j + S_{i-2}^j) - \\ & - \frac{\mu(\delta t)^2}{\delta x}\sum_{k=1}^{n-1} Q_{ik}(S_{k+1}^j - S_{k-1}^j) - \frac{2\mu Q_{in}(\delta t)^2}{\delta x}(S_n^j - S_{n-1}^j) - \\ & - \mu\delta t\sum_{k=1}^{n} Q_{ik}(S_k^j - S_k^{j-1} + S_{k-1}^j - S_{k-1}^{j-1}) + \mu\alpha^j(\delta t)^2\sqrt{\frac{n-i}{i}}, \end{aligned} \tag{38}$$

where S_i^j denotes the numerical approximation to $S(x_i, t_j)$, $\alpha(t_j)$ is abbreviated by α^j and Q_{ik} is given by (21).

Equation (38) is imposed for $i = 0, 1, \ldots, n$ and the boundary conditions are used to eliminate the fictitious points outside this region. Following the method used to eliminate to fictitious mesh points in Section 3.2, the discretisation for $i = 1$ is

$$\begin{aligned} S_1^{j+1} &= 2S_1^j - S_1^{j-1} - \frac{\gamma(\delta t)^2}{(\delta x)^4}(S_3^j - 4S_2^j + MS_1^j) - \\ &\quad - \frac{\mu(\delta t)^2}{\delta x}\sum_{k=1}^{n-1} Q_{1k}(S_{k+1}^j - S_{k-1}^j) - \frac{2\mu Q_{1n}(\delta t)^2}{\delta x}(S_n^j - S_{n-1}^j) - \\ &\quad - \mu\delta t\sum_{k=1}^{n} Q_{1k}(S_k^j - S_k^{j-1} + S_{k-1}^j - S_{k-1}^{j-1}) + \mu\alpha^j(\delta t)^2\sqrt{n-1}, \end{aligned} \tag{39}$$

where $M = 5$ for the hinged flag and $M = 7$ for the clamped flag. Similarly, both $i = n - 1$ and $i = n$ may be substituted in (38). The boundary conditions may now be used to eliminate S_{n+1}^j and S_{n+2}^j to give, for $i = n - 1$

$$\begin{aligned} S_{n-1}^{j+1} &= 2S_{n-1}^j - S_{n-1}^{j-1} - \frac{\gamma(\delta t)^2}{(\delta x)^4}(-2S_n^j + 5S_{n-1}^j - 4S_{n-2}^j + S_{n-3}^j) - \\ &\quad - \frac{\mu(\delta t)^2}{\delta x}\sum_{k=1}^{n-1} Q_{n-1,k}(S_{k+1}^j - S_{k-1}^j) - \frac{2\mu Q_{n-1,n}(\delta t)^2}{\delta x}(S_n^j - S_{n-1}^j) - \\ &\quad - \mu\delta t\sum_{k=1}^{n} Q_{n-1,k}(S_k^j - S_k^{j-1} + S_{k-1}^j - S_{k-1}^{j-1}) + \frac{\mu\alpha^j(\delta t)^2}{\sqrt{n-1}} \end{aligned} \tag{40}$$

and for $i = n$

$$\begin{aligned} S_n^{j+1} &= 2S_n^j - S_n^{j-1} - \frac{\gamma(\delta t)^2}{(\delta x)^4}(S_n^j - 2S_{n-1}^j + S_{n-2}^j) - \\ &\quad - \frac{\mu(\delta t)^2}{\delta x}\sum_{k=1}^{n-1} Q_{nk}(S_{k+1}^j - S_{k-1}^j) - \frac{2\mu Q_{nn}(\delta t)^2}{\delta x}(S_n^j - S_{n-1}^j) - \\ &\quad - \mu\delta t\sum_{k=1}^{n} Q_{nk}(S_k^j - S_k^{j-1} + S_{k-1}^j - S_{k-1}^{j-1}). \end{aligned} \tag{41}$$

Equations (39–41) along with Equation (38) for $i = 2, 3, \ldots, n - 2$ permit the calculation of S_i^{j+1} for $i = 1, 2, \ldots, n$ for a hinged or clamped flag. The initial condition used here is that the flag is initially at rest, *i.e.* $S_t(x, 0) = 0$, which gives $S_i^1 = S_i^0$. The initial flag shape, S_i^0, is computed by means of the numerical procedure of Section 3.2 for the angle of incidence α^0.

5.2.1. *Von Neumann numerical stability analysis*

In order to execute the numerical scheme described above, it is necessary to quantify the relationship between the time step δt and the spatial step size δx. To derive the *exact* Courant number for the scheme the singular integral terms must be accounted for and this leads to great difficulties. A simpler alternative is to perform standard Von Neumann stability analysis on the reduced equation

$$S_{tt} + \gamma S_{xxxx} = 0, \tag{42}$$

arguing that, under normal circumstances, the stability of the scheme is governed largely by the behaviour of the highest order derivatives of S. When (42) is discretised according to the proposed scheme we find that

$$\frac{S_i^{j+1} - 2S_i^j + S_i^{j-1}}{(\delta t)^2} = -\frac{\gamma}{(\delta x)^4}(S_{i+2}^j - 4S_{i+1}^j + 6S_i^j - 4S_{i-1}^j + S_{i-2}^j).$$

Using standard Von Neumann stability analysis (see, for example [16, Chapter 3]), we obtain the condition for numerical stability as

$$0 < \frac{\gamma(\delta t)^2}{(\delta x)^4}(1 - \cos(a\delta x))^2 < 1$$

for all real a. The stability requirement for the scheme is thus that the 'Courant number' $\mathcal{C} = 4\gamma(\delta t)^2/(\delta x)^4$ must satisfy

$$\mathcal{C} < 1. \tag{43}$$

Although this analysis may be criticised on the grounds that it is not exact, we note that in all numerical calculations that were performed, (43) was confirmed; for small Courant numbers stability was preserved but accuracy was compromised, whilst for Courant numbers greater than unity numerical instability ensued.

The stability requirement (43) highlights a major drawback of using an explicit method to solve (10). Since for a given flag γ is fixed, for a given number of spatial mesh points δt must be chosen so that (43) is satisfied. However, the Courant number increases rapidly as n increases and thus an extremely small time-step must be used. For example, to execute a procedure for $\gamma = 1$ and $n = 500$ up to $t = 4$ requires 2×10^6 time-steps, which is computationally expensive. Clearly, a compromise must be reached and hence $n = 100$ was used for the computational examples presented below. Calculations were also performed for larger values of n up to $n = 1000$; agreement between these experiments and the results for $n = 100$ was invariably excellent.

5.2.2. *Numerical results for a hinged flag*

Two sets of results are presented here for a hinged flag; the same $\alpha(t)$ was used for both, but the values of γ and μ varied between the two cases. The angle of incidence $\alpha(t)$ was given by

$$\alpha(t) = \begin{cases} -0{\cdot}25 & t < 0 \\ t - 0{\cdot}25 & 0 \le t \le 0{\cdot}5. \\ 0{\cdot}25 & t > 0{\cdot}5 \end{cases} \tag{44}$$

One of our main interests in this example was to determine whether the flag converged to the steady solution for $\alpha = 0{\cdot}25$ as $t \to \infty$ or some other motion ensued instead.

For $t \le 0$ we have $S(x, 0) = -0{\cdot}25x$ since the flag is aligned with the outer flow and the corresponding steady solution for $\alpha = 0{\cdot}25$ is a reflection of this initial solution about the x-axis. The easiest way to view the results is to produce an animation of the flag motion, and this may easily be done. For the purposes of the present study, however, the most instructive quantity to plot is the position of the trailing edge of the flag as a function of time. For unstable flags we might expect to see wild oscillations. It should be noted though that an absence of such behaviour need not necessarily indicate convergence or stability since it is possible

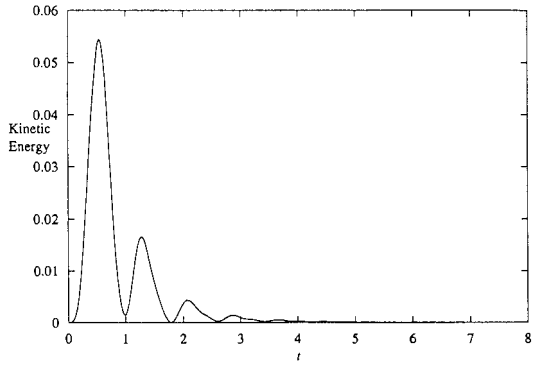

Figure 9. Kinetic energy of the hinged flag with $\gamma = 0{\cdot}2$ and $\mu = 7$.

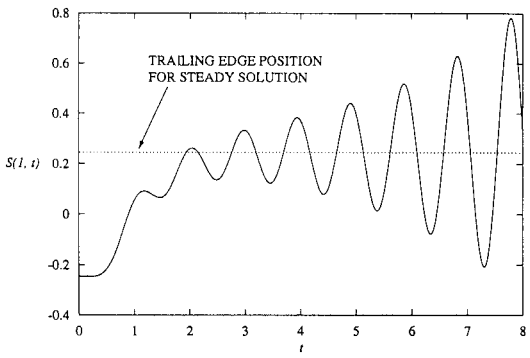

Figure 10. $S(1, t)$ for the hinged flag with $\gamma = 0{\cdot}2$ and $\mu = 3$.

that the trailing edge might remain stationary whilst the rest of the flag oscillates wildly. We therefore additionally examine the kinetic energy of the flag, defined as

$$\mathcal{K} = \frac{1}{2}\int_0^1 S_t^2 \, \mathrm{d}x,$$

arguing that a decay in kinetic energy indicates that the flag is converging to a solution.

Figure 8 shows how $S(1, t)$ varies with time for a flag with $\gamma = 0{\cdot}2$, $\mu = 7$. Results were calculated using a time increment of $\delta t = 1{\cdot}1 \times 10^{-4}$ (so that $\mathcal{C} = 0{\cdot}968$). The location of the trailing edge of the flag for the steady case where $\alpha = 0{\cdot}25$ is also plotted (broken line).

We observe that, when the angle of incidence ceases to change (at $t = 0{\cdot}5$), the trailing edge has hardly deviated from its initial position. Subsequently, however, the flag moves rapidly towards the steady ($\alpha = 0{\cdot}25$) solution via an oscillatory motion, which decays in amplitude and seems to have a constant period. The kinetic energy (plotted in Figure 9) confirms that the convergent behaviour of the trailing edge applies to the flag as a whole. This is in accordance with the results of the linear stability analysis presented in Figure 6. Analysis of successive flag shapes reveals further that, as one might expect, the outer flow is hardly able to influence the curvature of the flag in this case and the flag shapes resemble a succession of straight lines.

We now carried out a run that was identical to the previous case, save for the fact that $\mu = 3$ (a heavier flag). According to the linear stability results shown in Figure 6, this case should be unstable. The trailing edge position $S(1, t)$ is shown in Figure 10. As in the previous case, the flag has hardly deviated from its initial position by the time the angle of incidence ceases to change at $t = 0{\cdot}5$. Moreover, the deviation that *has* been experienced is smaller in this case. This is to be expected as the flag is heavier. An oscillatory motion then ensues. Although the trailing edge again oscillates about $S = 0{\cdot}25$ (with a seemingly constant period), the motion is evidently unstable, agreeing with the previous linear stability results. In order to illustrate the motion of the flag, Figure 11 shows flag shapes, plotted at times when the trailing edge is at a local maximum on Figure 10. The shapes in this case may be thought of as being 'first order' unstable modes as they possess curvature of constant sign. At about $x = 0{\cdot}7$ there exists a point on the flag that is virtually stationary. The flag on either side of this point moves

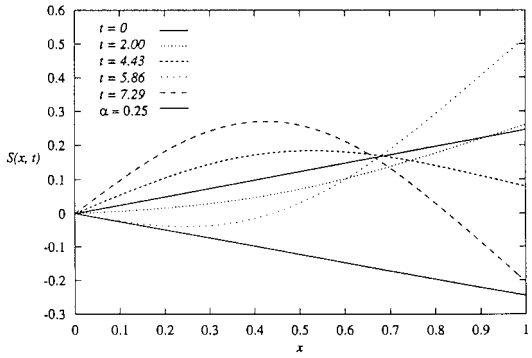

Figure 11. Hinged flag shapes with $\gamma = 0{\cdot}2$ and $\mu = 3$.

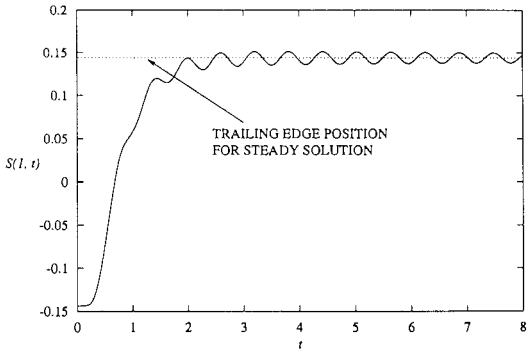

Figure 12. $S(1, t)$ for the clamped flag with $\gamma = 0{\cdot}2$ and $\mu = 7$.

in opposite directions. The kinetic energy for this case was also examined; as expected, it increased with time.

In this case an increase in the mass of the flag changes the motion of the flag from being stable to unstable. This is due to the fact that the outer flow, whilst able to overcome the inertia of the flag in the $\mu = 7$ case, is unable to do so when $\mu = 3$. The inertia of the flag therefore increases as time advances and the flag is unstable. Further numerical experiments showed that increasing the mass still further produced a stable motion where the flag moved slowly and monotonically towards the final solution. For very small values of μ the position of the flag remains virtually unchanged. This is because the outer flow is unable to impart a sufficient force to move such a massive flag. This marginally stable behaviour may be expected on physical grounds and is analysed in [8].

For smaller values of γ, the marginal stability diagram Figure 6 predicts second and (for small enough γ) higher order unstable modes. The existence of these modes may be confirmed by numerical calculations.

5.2.3. *Numerical results for a clamped flag*

Numerical experiments with identical parameter values to the hinged case were also carried out for a clamped flag.

Figure 12 plots $S(1, t)$ for a clamped flag with $\gamma = 0{\cdot}2$ and $\mu = 7$ (and $\alpha(t)$ given by (44)). Again, the position of the trailing edge of the steady solution is also plotted. As implied by Figure 7, the motion in this case is stable; the trailing edge moves towards its final position and then oscillates around this solution with a (fairly weakly) decaying amplitude. The flag is confirmed as being stable by the plot of the kinetic energy (presented in Figure 13) which decreases in magnitude as time advances.

The kinetic energy of this flag is much smaller in magnitude than that of the corresponding hinged flag which is given in Figure 9. This is because the deviation from the x-axis of steady hinged solutions is greater than that for a clamped flag and therefore the hinged flag has further to move before reaching the steady solution for $\alpha = 0{\cdot}25$. However, the hinged flag converges to the final steady solution more rapidly than the clamped flag. Presumably this is because a hinged flag offers no resistance to the outer flow, being able to freely pivot at its leading edge. In contrast, a clamped flag resists the aerodynamic forces imparted by the outer flow and is

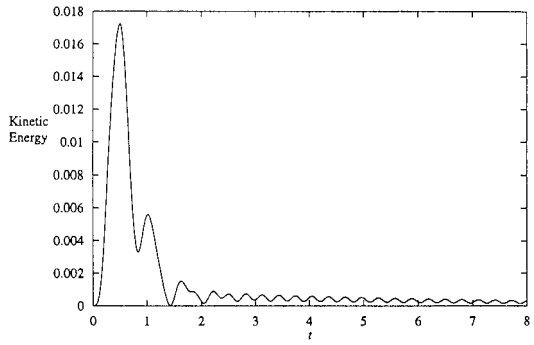

Figure 13. Kinetic energy of the clamped flag with $\gamma = 0{\cdot}2$ and $\mu = 7$.

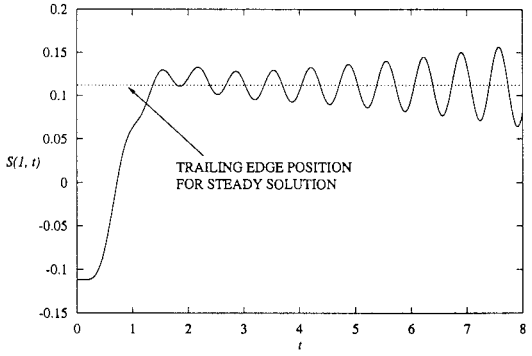

Figure 14. $S(1, t)$ for the clamped flag with $\gamma = 0{\cdot}2$ and $\mu = 3$.

forced to bend in order to adopt its final steady solution. This resistance causes the flag to oscillate around the final steady solution both with a smaller period and a weaker decay than the hinged flag.

Figure 14 shows $S(1, t)$ for a heavier clamped flag with $\gamma = 0{\cdot}2$ and $\mu = 3$ along with the position of the trailing edge of the flag for the final steady solution for $\alpha = 0{\cdot}25$. The motion is clearly unstable, agreeing again with the predictions of Section 4. The rate of divergence is slower than that of the corresponding hinged flag shown in Figure 10; presumably this is again due to the fact that the clamped flag resists the aerodynamic forces imparted on it whereas the hinged flag moves more freely under the influence of the outer flow.

6. Conclusions

A mathematical model for a flag of finite mass with bending stiffness has been proposed in this paper by coupling beam theory and thin aerofoil theory. The steady solutions for a flag hinged at its leading edge are trivial in that, as might be expected, the flag aligns with the outer flow. However, steady solutions for a flag that is clamped at its leading edge depend upon both the angle of incidence and the ratio of the outer flow momentum to the flexural rigidity of the flag.

Linear stability analysis of the unsteady flag equation has been used to quantify how hinged and clamped flags behave when subjected to time-dependent perturbations. The resulting quadratic eigenvalue problem was transformed to a standard eigenvalue problem, thus enabling standard numerical methods to be used. The eigenvalue problem has been solved for various values of γ^* and μ^* to construct the marginal stability curves for hinged and clamped flags. These curves reveal that a flag is stable for $\gamma^* > 1{\cdot}88$ (hinged flag) and for $\gamma^* > 0{\cdot}99$ (clamped flag). In these cases the flag has sufficient stiffness to be largely unaffected by the outer flow.

To confirm the results of the stability analysis, a numerical method was proposed for the full unsteady flag equation; as far as we are aware, very few schemes have successfully been used to compute numerical solutions to partial singular integro-differential equations. The scheme was capable of predicting both stable and unstable flag motion, and in each case the results agreed exactly with our previous stability analysis. The solutions in the lower unstable

regions of the marginal stability diagram were found to be first-order mode solutions. For sufficiently small flexural rigidity and mass there exist higher-order mode solutions.

The model could be extended in a number of ways if desired. The effects of gravity, flag porosity and hinge resistance could all easily be included, and viscous drag could be accounted for by the inclusion of a shear force term. The basic form of the governing partial singular integro-differential equation would not change a great deal, however, and the proposed numerical methods would still be largely applicable.

Acknowledgements

MPP acknowledges the financial assistance of the EPSRC for a studentship during which this work was carried out.

References

1. M. Haselgrove, *Stability Properties of Two-Dimensional Sail Configurations*. PhD thesis, University of Adelaide (1973) 223 pp.
2. T.R.B. Lattimer, *Singular Partial Integro-Differential Equations Arising in Thin Aerofoil Theory*. PhD thesis, University of Southampton (1996) 159 pp.
3. M. Bäcker, H. Neunzert and S. Younis, The Fluttering of fibres in airspinning processes. In: H. Wacker and W. Zulehner (eds), *Proceedings of the Fourth European Conference on Mathematics in Industry*. Stuttgart: B.G. Teubner and Dordrecht: Kluwer Academic Publishers (1991) pp. 197–205.
4. A. Kornecki, E.H. Dowell and J. O'Brien, On the aeroelastic instability of two-dimensional panels in uniform incompressible flow. *J. Sound Vibr.* 47 (1976) 163–178.
5. L.K. Shayo, The stability of cantilever panels in uniform incompressible airflow. *J. Sound Vibr.* 68 (1980) 341–350.
6. L. Huang, Flutter of cantilevered plates in axial flow. *J. Fluids Struct.* 9 (1995) 127–147.
7. L. Meirovitch, *Elements of Vibration Analysis*. New York: McGraw-Hill (1975) 495 pp.
8. W. Frederiks, H.C.J. Hilberink and J.A. Sparenberg, On the Kutta condition for flow along a semi-infinite elastic plate. *J. Eng. Math.* 20 (1986) 27–50.
9. K. Voelz, Profil und Auftrieb eines Segels. *Zeit. Angew. Math. Mech.* 30 (1950) 301–317.
10. B. Thwaites, The aerodynamic theory of sails. *Proc. R. Soc. London A* 261 (1961) 402–422.
11. N.I. Muskhelishvili, *Singular Integral Equations*. Groningen: Noordhoff (1953) 447 pp.
12. L.M. Milne-Thomson, *Theoretical Aerodynamics*. London: Macmillan (1952) 414 pp.
13. M.P. Pope, *Mathematical Modelling of Unsteady Problems in Thin Aerofoil Theory*. PhD thesis, University of Southampton (1999) 169 pp.
14. T. Brooke Benjamin, Internal waves of permanent form of fluids of great depth. *J. Fluid Mech.* 29 (1967) 559–592.
15. H. Ono, Algebraic solitary waves in stratified fluids. *J. Phys. Soc. Japan* 39 (1975) 1082–1091.
16. G.D. Smith, *Numerical Solution of Partial Differential Equations: Finite Difference Methods*. Oxford Applied Mathematics and Computing Science Series. Oxford: Oxford University Press (1978) 304 pp.